Investigation of the Magnetosphere-Solar wind interaction using an artificial neural network

Mehdi Heidari, Doctoral student, Faculty of Physics, Yazd University, Yazd, IRAN

Seyed Majid Mir Rokni, Assistant Professor, Retired, Faculty of Physics, Yazd University, Yazd, IRAN

Abstract:

The significant variations in solar and magnetic parameters during peak solar activity periods necessitate detailed analysis to understand the interactions between the solar wind and the magnetosphere. The present research investigated the impact of various solar wind parameters on the Polar Cap (PC) magnetic activity index. The primary objective of this research is to identify and analyze the relationships between solar wind speed (V_{SW}), solar wind dynamic pressure (P_{SW}), and the interplanetary electric activity index (AE) with the PC index. A multilayer perceptron (MLP) artificial neural network model has been utilized to explore these relationships. Identifying and predicting complex nonlinear relationships between the input variables and the PC index is the distinctive feature of the model. The dataset used in this research was obtained from Defense Meteorological Satellite Program (DMSP) satellites and includes V_{SW}, P_{SW}, and AE parameters during periods of peak solar activity in 2002 and 2014. These data were used to analyze the temporal and seasonal variations of the PC index.

The results indicate that artificial neural network models can effectively predict the PC index, and a strong correlation between the PC index and the input parameters, particularly in the first half of the years under research, has been observed. The results show the high potential of machine learning models to analyze and predict geomagnetic phenomena, which can improve forecasting and management of geomagnetic disturbances, and serve as a suitable alternative to classical models.

Keywords: Solar wind, Artificial Neural network, Polar Cap, Machine learning, Magnetosphere

Introduction:

The solar physics system is vast and contains numerous parameters influencing Earth's magnetosphere. When assessing the impact of the magnetosphere on the ionosphere, these parameters become even more complex. The Polar Cap (PC) magnetic activity index, by definition, corresponds to the intensity of magnetic disturbances in the polar cap and is calibrated against the effective interplanetary Electric Field (EF) (Kan & Lee, 1979). The PC index reflects the energy transferred from the solar wind to the magnetosphere and is strongly controlled by solar wind parameters such as the interplanetary electric field (E_{KL}) (Troshichev & Sormakov, 2015).

One crucial component within the magnetosphere is the ring current, an electric current that flows around the Earth in the inner magnetosphere near the Earth's magnetic equator. The ring current generated by energetic ions in the solar wind plays a main role in weakening the Earth's magnetic field in equatorial regions during geomagnetic storms. The ring current can also interact with other parameters, such as the Interplanetary Magnetic Field (IMF) components, to influence the intensity of magnetic disturbances(Kozyra & Nagy, 1991).

The ring current injection time **(τ)** represents the period during which the ring current in Earth's magnetosphere intensifies. This process is initiated by the entry of charged particles and high-energy protons from the solar wind into the magnetosphere, transferring energy to this region. Specifically, ring current injection occurs when the southward component of the interplanetary magnetic field (B_Z) is negative, which allows Earth's magnetic field to couple with the interplanetary field and enhances the transfer of solar wind energy into the magnetosphere. Under such conditions, the interplanetary electric field VBs (which is the product of solar wind speed and the southward B_Z component) channels solar wind

energy into the magnetosphere, resulting in increased injection of plasma and charged particles into Earth's magnetic orbits, thereby strengthening the ring current(O'Brien & McPherron, 2000).

The primary driving parameter in the solar wind-magnetosphere interaction is the southward component (B_Z) of the IMF. At the same time, the IMF's B_Y component, which drives the ring current, also plays a key role in this interaction, with its effects typically assumed to be independent of its sign.

For a constant level of the solar wind, the interplanetary magnetic field (IMF) B_Y significantly influences the magnetospheric convection and plasma dynamics. During the northern hemisphere's summer, $B_Y<0$ enhances the flux of energetic protons and the rate of ring current growth compared to $B_Y>0$. Conversely, in the winter, $B_Y>0$ shows stronger effects on ring current development and plasma convection. This seasonal modulation reflects the sensitivity of magnetospheric dynamics to the direction of the IMF B_Y, which governs magnetic reconnection and energy transfer processes. The results indicate that B_Y modulates magnetospheric convection and plasma transport within the inner magnetosphere(Holappa & Buzulukova, 2022; Rice et al., 2024).

Interplanetary shocks represent sudden and strong enhancements in the solar wind dynamic pressure (P_{SW}), which compress the Earth's magnetosphere, manifesting as a geomagnetic field impulse. If this shock coincides with a magnetic storm, it is considered a sudden storm commencement; otherwise, it is simply an impulse. The pressure waves propagated in the magnetosphere affect magnetic field oscillations and the flux of energetic particles in the geosynchronous orbit(Lee et al., 2004).

Compressional waves in the magnetosphere, often generated by sudden changes in the dynamic pressure of the solar wind, refer to pressure oscillations that propagate through the magnetosphere. These waves induce magnetic field oscillations and variations in the flux of energetic particles in the geosynchronous orbit. This process significantly impacts the stability and distribution of particles in these orbits, leading to wide-ranging effects on the structure and functionality of the magnetosphere(Yamamoto et al., 2024).

The PC index correlates with P_{SW} variations (either increasing or decreasing). Discrepancies between the behavior of P_{SW} and PC become apparent as E_{KL} and P_{SW} diverge (Troshichev & Sormakov, 2019). The relationship between magnetospheric dynamics and IMF orientation was qualitatively discovered in the 1960s (Dungey, 1961), it was observed that when the IMF with a southward direction reaches Earth, magnetic reconnection between the Earth's magnetic field and the IMF occurs. Consequently, the Earth's magnetic field can directly connect to the IMF, allowing high-energy particles from the solar wind to enter the magnetosphere along magnetic field lines. If this process continues for several hours both the magnetic field and plasma within the magnetosphere will be severely disrupted by the solar wind, leading to a geomagnetic storm (Gonzalez et al., 1994).

Studies on the effect of solar wind dynamic pressure on the collapse and injection of the ring current, based on solar wind and the geomagnetic index, show that ring current injection increases when the magnetosphere is compressed by solar wind dynamic pressure (Wang et al., 2003). The physical analysis of the convection pattern of hot ions forming the ring current suggests that the position of the ring current is controlled by the interplanetary electric field VB_S during ring current injection. It should be noted, however, that injection into the ring current occurs not only during southward IMF intervals but also for northward IMF intervals, although the latter is much weaker and depends on the solar wind-magnetosphere energy coupling parameter (Akasofu, 1981).

In empirical models developed for ring current collapse and injection, the solar wind dynamic pressure is critical in controlling ring current injection, particularly during strong magnetic storms. The strength of ring current injection is proportional to the solar wind dynamic pressure with a power index of 0.2 during southward IMF intervals. Thus, ring current injection increases when the magnetosphere is compressed by high solar wind dynamic pressure (Wang et al., 2003).

The main objective of this research is to investigate the impact of solar wind parameters on the Polar Cap (PC) magnetic activity index and to evaluate the effectiveness of multilayer perceptron (MLP) artificial neural network models in predicting this index. Additionally, this research aims to identify and analyze the complex relationships between solar wind speed (V_{SW}), solar wind dynamic pressure (P_{SW}), and the interplanetary electric activity index (AE) with the PC index during periods of peak solar activity in 2002 and 2014. The findings of this research can contribute to improving predictive models and the management of geomagnetic disturbances, aiding scientists in better understanding the complex interactions between the solar wind and the magnetosphere.

2- Research Methodology

This numerical research is designed as a modeling approach using a multilayer perceptron (MLP) neural network. The solar wind parameters, which determine the efficiency of the solar wind-magnetosphere-ionosphere coupling were examined using the MLP artificial neural network. In this research, we predicted the Polar Cap (PC) magnetic activity index, which indicates magnetic disturbances in the polar cap, by utilizing solar wind speed (V_{SW}), solar wind dynamic pressure (P_{SW}), and the ionospheric response to solar wind pressure pulses, represented by the AE index.

2.1 Equations and Modeling

The PC magnetic activity was modeled using several key equations describing the relationships between solar wind parameters and the PC index. These equations contribute to a better understanding of how these parameters influence magnetospheric behavior and form the basis for the numerical analyses conducted in this research.

2.1.1 Interplanetary Electric Field (E_{KL})

One of the most important parameters in geophysical analyses is the interplanetary electric field (E_{KL}), which significantly affects the energy transfer from the solar wind to the magnetosphere. The E_{KL} electric field is determined by the Kan and Lee formula:

$$E_{KL}=V_{SW}(B_Y{}^2+B_Z{}^2)^{\frac{1}{2}}\sin^2\frac{\theta}{2} \quad (1)$$

In this equation, EKL represents the interplanetary electric field, V_{SW} is the solar wind speed, B_Y and B_Z are the components of the interplanetary magnetic field (IMF), and θ is the angle between the transverse component of the IMF and the geomagnetic dipole.

2.1.2 Solar Wind Dynamic Pressure (P_{SW})

Predicting the PC index requires modeling the impact of solar wind dynamic pressure on the magnetosphere. Solar wind dynamic pressure is generated by the collision of solar wind particles with the magnetospheric boundary, influencing the density of the magnetosphere. The relationship between the PC index and solar wind dynamic pressure (P_{SW}) is expressed as follows:

$$PC=\alpha\times Psw^{\beta} \quad (2)$$

In this equation, PC is the Polar Cap magnetic activity index, P_{SW} is the solar wind dynamic pressure, and α and β are empirical parameters derived from observational data. This equation empirically models the effect of dynamic pressure on PC index variations(Kivelson & Russell, 1995).

2.1.3 Ring Current Injection Time (τ)

Another critical aspect of magnetospheric analysis is examining the ring current injection time (τ), which is influenced by the interplanetary magnetic field (IMF).

The ring current injection time (τ) represents the period during which the ring current in Earth's magnetosphere intensifies. This process begins with the entry of charged particles, particularly energetic protons from the solar wind, into the magnetosphere and the subsequent transfer of energy to this region. Specifically, the ring current injection occurs when the southward component of the interplanetary magnetic field (B_Z) is negative. Under these conditions, a process known as **magnetic reconnection** occurs at the magnetopause, facilitating the transfer of energy from the solar wind into the magnetosphere(O'Brien & McPherron, 2000; Pfau-Kempf et al., 2024).

Interplanetary electric fields, such as VB_S, play a crucial role in this process by enhancing the energy transfer from the solar wind to the magnetosphere. Following this reconnection, more plasma and charged particles are injected into Earth's magnetic field lines, leading to an intensification of the ring current.

The ring current is a type of electric current that flows in the inner magnetosphere near the magnetic equator and plays a critical role in geomagnetic variations. Its injection and intensification, particularly during geomagnetic storms, result in significant changes in the strength of Earth's magnetic field in equatorial and polar regions. Consequently, it plays a vital role in geomagnetic phenomena and space weather interactions(Feldstein et al., 1984; Hashimoto et al., 2002).

The following equation is used for modeling this time:

$$\tau=2.40e^{9.74/(4.69+VB_s)} \quad (3)$$

In this relation, VB_S is measured in mV/m. Here, VB_S is defined as:

$$VB_S=\begin{cases}|VB_Z| & B_Z<0\\ 0 & B_Z>0\end{cases} \quad (4)$$

Here V represents the solar wind speed, and B_Z is the Z-component of the interplanetary magnetic field (IMF) in the geocentric solar magnetic (GSM) coordinate system. Northward IMF (positive B_Z), significant displacement in the magnetosphere is not expected, and VB_S is assumed to be 0. Plasma is only injected into the ring current under the influence of a southward IMF component, while the dawn-dusk electric field component in the interplanetary environment remains below 0.5 mV/m³(O'Brien & McPherron, 2000).

Interplanetary electric fields play a crucial role in the interaction between the solar wind and the magnetosphere. In this study, both E_{KL} and VB_S are utilized to represent different aspects of the interplanetary electric field. E_{KL} offers a comprehensive and precise calculation by considering the magnetic field's angular component, while VB_S provides a simplified proxy for energy coupling under specific southward B_Z conditions(Boteler, 2019; Tepke, 2019).

Ring current injection time (τ) is a critical parameter influenced by the southward component of the interplanetary magnetic field B_Z , where increased energy transfer leads to enhanced ring current intensity. VB_S, focusing on the B_Z component, serves as a simplified metric for assessing energy transfer and ring current injection under specific conditions, whereas E_{KL} is more suitable for broader analyses of interplanetary energy fields(Troshichev et al., 2012).

2.2 Dataset and Sources

The dataset used in this research was obtained from the Defense Meteorological Satellite Program (DMSP). These satellites record solar wind parameters and ionospheric responses at one-minute intervals, enabling researchers to analyze temporal variations in these parameters with high precision. The dataset includes solar wind speed (V_{SW}), solar wind dynamic pressure (P_{SW}), and the interplanetary electric activity index (AE). The years analyzed in this research are 2002 and 2014 characterized by peak solar activity. The dataset includes daily average and instantaneous values of V_{SW}, P_{SW}, and AE, which play a crucial role in

magnetic analyses and are divided into the first and second six months to examine seasonal variations. The dataset was normalized within the range of -1 to 1. This normalization allows the neural network model to train more efficiently and provide more accurate predictions.

2.3 Tools and Materials

A multilayer perceptron (MLP) neural network was employed to predict the PC index. The model was implemented using MATLAB version 2019. The multilayer perceptron is a feedforward artificial neural network composed of several layers of neurons with activation functions. It typically consists of three layers: an input layer, one or more hidden layers, and an output layer. Each neuron uses a nonlinear activation function to mathematically learn the correct representation of the dataset (Wallace et al., 2022). One input layer, three hidden layers with approximately 350 neurons each, and one output layer were used. A sigmoid activation function was employed for the neurons, optimized after testing several mathematical functions.

2.4 Data Analysis Methods

The dataset was analyzed using a multilayer perceptron neural network. The learning rate of the model was set at 1000, and the dataset was randomly divided into a training subset (70%) and a test subset (30%). The perceptron model was trained to predict the PC index, and the results were evaluated using the mean squared error (MSE). Each experiment was repeated five times, and the average results were presented in the relevant tables. This method ensures the stability and reliability of the results. The training subset was used to optimize hyperparameters and build the model, while the test subset was used to evaluate the model's performance. The model accuracy was assessed using

the mean squared error (MSE). Techniques like regularization and dropout were employed to prevent overfitting.

2.5 Neural Network Configuration

The neural network consists of an input layer with three neurons for the parameters V_{SW}, P_{SW}, and AE, three hidden layers with approximately 350 neurons in each layer, and an output layer with a single neuron for the PC index. Sigmoid activation functions were chosen for the hidden layers to enhance the model's capability in modeling nonlinear relationships. The weights and biases were randomly initialized and optimized using the backpropagation algorithm.

3 Measurement, Observation, and Calculation

The input dataset, referred to as features here, includes solar wind speed (V_{SW}), solar wind dynamic pressure (P_{SW}), and the ionospheric response to solar wind pressure pulses, represented by the AE index. These indices play a significant role in the solar wind energy transferred to the magnetosphere, represented by the PC index. It can be observed that the annual average PC values are closely correlated with the selected solar wind parameters, with a correlation coefficient of $R = 0.86$ for V_{SW}. In Addition, a correlation coefficient of $R = 0.97$ for the AE index indicates a strong relationship between the annual average PC and AE. The correlation coefficient between P_{SW} and PC is $R = 0.83$, which is substantial (Kan & Lee, 1979).

The dataset used in this research, comprising solar wind and PC index data, was sourced from the U.S. Defense Meteorological Satellite Program (DMSP), which collects extensive data that can reveal various ionospheric and magnetospheric states (T. Paul O'Brien, 2000).

As shown in Figure (1), 2002 and 2014 were selected for analysis due to the high incidence of solar storms and sunspot activity observed during these years.

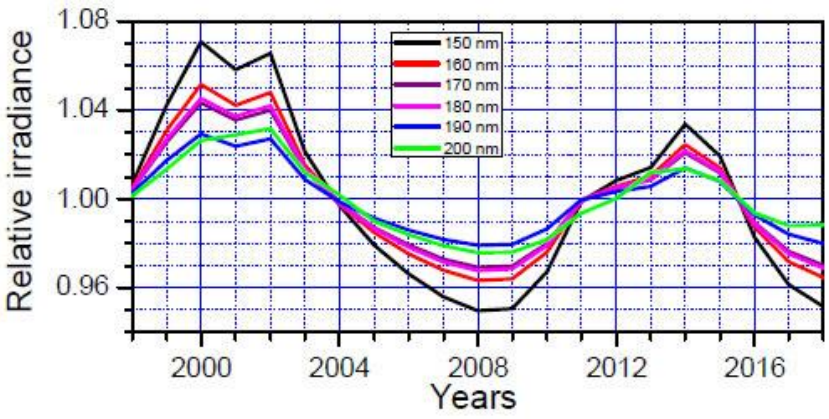

Figure 1: Solar activity during the years 1998-2018

Relative irradiance, as shown in Figure 1, reflects the variations in solar radiative energy reaching Earth's surface. This measure is closely related to sunspot numbers, which represent areas of strong magnetic activity on the Sun's surface that periodically appear and disappear during the solar cycle(Sedrati et al., 2024).

When sunspot numbers increase, solar radiative energy—or relative irradiance—also rises due to heightened solar activity. This correlation is particularly noticeable during solar maximum, when the Sun emits higher levels of energy. Sunspot numbers thus serve as indicators of solar activity and fluctuations in solar irradiance, as illustrated in Figure 1(Maghrabi & Alghamdi, 2024).

3.1 Data Preprocessing

Data preprocessing is a critical stage in any data analysis process, directly affecting the quality and accuracy of research results. Various data preprocessing steps were undertaken for statistical analysis and machine learning modeling.

3.2 Data Cleaning:

First, the raw dataset was examined to address potential issues such as missing data, invalid values, and obvious errors. For rows where more than 40% of the values are missing, the entire row was removed. If the missing values are less than this threshold, they were imputed using the nearest-neighbor approach depending on the data type(García et al., 2015). After handling missing data, the outliers were identified and removed using the Interquartile Range (IQR) method to obtain a valid dataset. In this method, outliers are detected and removed by dividing the sorted dataset into four quartiles: Q1, Q2, Q3, and Q4, with each quartile containing 25% of the sorted data. The IQR is the difference between Q3 and Q1:

$$LB = Q1 - 1.5\times(Q3 - Q1) \quad (5)$$

$$UB=Q3 + 1.5\times (Q3 - Q1) \quad (6)$$

Here, LB and UB are the lower and upper bounds for acceptable values, and any values outside this range are considered outliers and are removed from the dataset(Beer et al., 2010).

3.3 Normalization:

The dataset was normalized to ensure uniformity and comparability on an appropriate scale. This process involves converting the dataset to a common scale to reduce the impact of large variances across different scales(Han et al., 2022). To ensure the accuracy of the dataset, the input parameters were normalized using the Min-Max method. This range was selected to correctly encapsulate the PC index values, as the PC index contains both positive and negative values. In this method, a positive PC index indicates disturbed planetary conditions due to solar wind, while a negative PC index corresponds to calm planetary conditions(Troshichev et al., 2006). This normalization enhances the performance of the neural network model by ensuring that the dataset is uniformly used during the learning process. After outliers were removed and missing values corrected, the data were normalized. The collected data, sampled at a 1-minute interval, includes 289,000 data rows. Each year was divided into two six-month periods.

To implement and evaluate the multilayer perceptron (MLP) neural network model, MATLAB version 2019 was utilized. The neural network model consists of an input layer, three hidden layers with approximately 350 neurons each, and an output layer. The sigmoid function was used for the neurons in this network, which was selected as the optimal function after testing several mathematical functions. During the training process, various parameters, including weights and biases, were iteratively adjusted and optimized.

A learning rate of 1000 was selected to keep the number of iterations consistent across each experiment. The database used was randomly split into training and testing subsets. The training subset consisted of 70% of the entire dataset, while the validation subset included the remaining 30%. The training dataset was randomly selected from all points in the database to optimize hyperparameters and build the perceptron model effectively. The validation dataset was also used for predicting the model's performance and assessing it.

At each stage, the model's error is calculated and reported using the Mean Squared Error (MSE) metric. The Mean Squared Error (MSE) is a key metric for evaluating model accuracy by measuring the difference between predicted and actual values. This metric calculates error by squaring each sample's deviation and then averaging these squared errors, where lower MSE values indicate higher model accuracy(Goodfellow, 2016). Regularization is a technique used to reduce model complexity and prevent overfitting. By adding a regularization term to the loss function, the model is encouraged to find solutions with smaller weights, thus enhancing generalizability. The Dropout technique is another method to prevent overfitting, wherein some neurons are randomly deactivated during the learning process. This approach helps the model avoid excessive reliance on specific features, resulting in improved generalization capabilities(Srivastava et al., 2014).

4. Analysis:

The impact of solar wind parameters on the Polar Cap (PC) index during periods of peak solar activity in 2002 and 2014 was investigated using a multilayer perceptron (MLP) neural network. To obtain better results and avoid system-related errors, each experiment was repeated five times under identical conditions, and the results are presented in the following tables:

Table ' : The results of five iterations of the Perceptron model for the first semester of 2002.

Repetition	Linear Regression (reg)	Training Dataset Error (ErrorTR)	MSE Test Dataset (MSETS)	MSE Training Dataset (MSETR)	Test Dataset Error (ErrorTS)
1	0.79991	2.738613	0.0032	0.003	2.828427
2	0.79912	2.738613	0.0032	0.003	2.828427

3	0.80979	2.692582	0.0032	0.0029	2.828427
4	0.80532	2.692582	0.003	0.0029	2.738613
5	0.80466	2.692582	0.0031	0.0029	2.783882
Average	0.80376	2.710995	0.00314	0.00294	2.801555

The results obtained from running the model five times for the first half of 2002 are presented in Table (1). As observed, the average linear regression coefficient between the PC index and the parameters AE, P_{SW}, and V_{SW} is 0.80376. The mean squared error (MSE) of the training and test datasets are 0.00294 and 0.00314, respectively. The average error for the training and test datasets is 2.710995 and 2.801555, respectively. These results indicate the model's satisfactory performance in the first half of 2002 and demonstrate a good correlation between the solar wind parameters and the PC index.

Table ۲ : The results of five iterations of the Perceptron model for the second semester of 2002.

Repetition	Test Dataset Error (ErrorTS)	Training Dataset Error (ErrorTR)	MSE Test Dataset (MSETS)	MSE Training Dataset (MSETR)	Linear Regression (reg)
1	4.330127	4.272002	0.0075	0.0073	0.77925
2	4.415588	4.301163	0.0078	0.0074	0.77494
3	4.358899	4.272002	0.0076	0.0073	0.77952
4	4.330127	4.272002	0.0075	0.0073	0.77814
5	4.387482	4.272002	0.0077	0.0073	0.77712
Average	4.364503	4.277834	0.0076	0.00732	0.77779

The results obtained from running the model five times for the second half of 2002 are presented in Table (2). As observed, the average linear regression coefficient between the PC index and the parameters AE, P_{SW}, and V_{SW} is 0.777794. The mean squared error (MSE) of the training and test datasets are 0.00732 and 0.00762, respectively. The average error for the training and test datasets is 4.277834 and 4.364503, respectively. These results indicate that the model's performance in the second half of 2002 is less favorable.

In Tables 1 and 2, the modeling results are presented separately for the first and second halves of the year to examine the correlation between solar wind parameters and the PC index. Specifically, Table 1 demonstrates higher correlations and better model performance in the first half of the year, as indicated by higher correlation coefficients and lower Mean Squared Error (MSE) values. These results highlight a strong relationship between the input parameters and the PC index during this period.

In contrast, Table 2, which corresponds to the second half of the year, shows a decrease in the correlation coefficient and an increase in MSE values. This indicates a reduction in correlation and model accuracy during this timeframe. These variations may be attributed to differences in seasonal conditions, ionospheric changes, and reduced solar activity in the second half of the year. Such factors lessen the influence of input parameters on the PC index, resulting in weaker correlations.

The higher correlation coefficient and lower error values in Table 1 suggest a stronger connection between the parameters and the PC index in the first half of the year. Conversely, the lower correlation coefficient and higher error values in Table 2 reflect a diminished connection in the second half. These variations may arise from seasonal factors and natural changes in magnetic and ionospheric conditions that affect the PC index.The findings suggest that the correlation between the PC index and the parameters AE, P_{SW}, and V_{SW} is stronger in the first half of the year compared to the second half. These results are consistent with those reported by O. A. Troshichev and colleagues in 2002(García et al., 2015).

Specifically, the correlation between the PC index and the parameters P_{SW} and V_{SW} during summer (denoted as PC_{SUMM}) is higher than in winter (denoted as PC_{WINT}). The multilayer perceptron (MLP) neural network accurately captured these results.

4.1 Validation with the 2014 Dataset

In this research, the MLP neural network model was validated to assess the accuracy and stability of predicting the Polar Cap (PC) magnetic activity index. The validation aimed to evaluate the model's ability to generalize and predict new data that it had not encountered during training. To emphasize the reliability of the results and validate the model, the 2014 dataset was used. This year was chosen due to its similarity in solar activity conditions to 2002.

The validation results, as presented in Tables 1 and 2 for the first and second semesters of 2002, respectively, show that the Perceptron model demonstrates higher correlation coefficients and lower Mean Squared Error (MSE) values in the first semester compared to the second semester. This indicates a stronger relationship between the input parameters (AE, PSW, and VSW) and the PC index during the first semester.

Similarly, the validation results for 2014, displayed in Tables 3 and 4 for the first and second semesters, confirm the consistency of the model's performance. Higher correlation coefficients and lower MSE values in Table 3 reinforce the model's capability to capture seasonal variations, aligning with the results observed in 2002. These findings validate the effectiveness of the MLP model in reliably predicting the PC index under different solar wind conditions.

Table ٣ : The results of five iterations of the Perceptron model for the first semester of 2014.

Repetition	Linear Regression (reg)	MSE	Error
1	0.81722	0.0121	5.5
2	0.81639	0.0122	5,226,800
3	0.82025	0.0120	4,772,250
4	0.81448	0.0124	5,677,640
5	0.81420	0.0124	5,677,640
Average	0.81651	0.0122	5,270,887

The results from the first half of 2014, presented in Table (3), indicate that the average linear regression coefficient is 0.816508, and the mean squared error is 0.01222. The average error is 5.270869. These results demonstrate a strong correlation between the PC index and the parameters AE, P_{SW}, and V_{SW} during the

first half of 2014, reflecting the model's effectiveness in capturing the relationships between solar wind parameters and the PC index during this period.

Table ٤ : The results of five iterations of the Perceptron model for the second semester of 2014.

Repetition	Linear Regression (reg)	MSE	Error
1	0.79521	0.0143	5,979,130.3
2	0.79141	0.0144	6.0
3	0.79156	0.0144	6.0
4	0.78915	0.0145	6,020,797.2
5	0.78975	0.0144	6,020,797.2
Average	0.79141	0.0144	6,004,144.1

The results obtained for the second half of 2014, as shown in Table (4), indicate that the average linear regression coefficient is 0.791416, the mean squared error (MSE) is 0.01442, and the average error is 6.004144. These results suggest a lower correlation between the PC index and the parameters AE, P_{SW}, and V_{SW} in the second half of 2014 compared to the first half.

These findings demonstrate that the neural network model was able to predict the PC index in 2014 with high accuracy. The higher correlation in the first half and its decrease in the second half align with the pattern observed in 2002, further emphasizing the validity and effectiveness of the model.

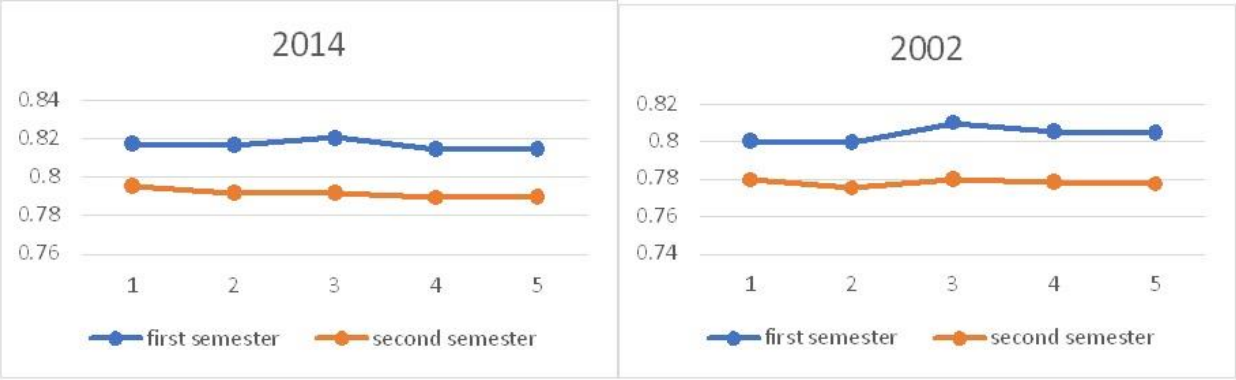

Figure 2: A comparison of the performance of the artificial neural network between the years 2002 and 2014, as well as a comparison of its performance during the first and second semesters(dmsp).

As illustrated in Figure (2), in both 2002 and 2014, the correlation between the PC index and the input parameters was higher in the first half of the year compared to the second half. This indicates that the model was able to identify similar patterns across different time periods. The results suggest that seasonal variations can have a significant impact on the correlation between the input parameters and the PC index. The stronger correlation in the first half of the year (summer) may be attributed to changes in solar activity and ionospheric conditions.

The repetition of experiments and averaging of results indicate the stability and accuracy of the model in predicting the PC index. This approach reduces random fluctuations and enhances confidence in the obtained results. Machine learning models, such as perceptron neural networks, not only increase the speed and accuracy of geophysical analyses but also produce results consistent with observational data and traditional models. This highlights the high capability of these models in analyzing complex and large datasets.

The model's ability to consistently recognize seasonal patterns and provide reliable predictions in different periods emphasizes the importance of advanced machine learning approaches in geophysical research. By leveraging these techniques, researchers can gain deeper insights into the interactions between solar wind and the magnetosphere, ultimately leading to improved prediction and management of geomagnetic disturbances.

5 Conclusion:

The main objective of the present research was to investigate the effect of solar wind parameters on the Polar Cap (PC) magnetic activity index during periods of peak solar activity in 2002 and 2014 and to evaluate the efficiency of multilayer perceptron (MLP) neural network models in predicting this index. The results indicate that artificial neural network models are powerful tools for analyzing and predicting geomagnetic phenomena.

Data analysis showed that the correlation between the PC index and the input parameters V_{SW}, P_{SW}, and AE in the first half of both years was higher than in the second half. This finding particularly indicates that the MLP model has accurately identified seasonal patterns. Higher solar activity and different ionospheric conditions in the first half could be the main reasons for this higher correlation. In the second half, the observed decrease in correlation could be related to seasonal changes and reduced solar activity.

The stability and high accuracy of the model in predicting the PC index were confirmed through repeated experiments and averaging the results. These methods reduced random fluctuations and increased confidence in the obtained results. On average, the linear regression and mean squared error (MSE) in the first half improved compared to the second half, indicating higher accuracy of the model in predicting the first half's dataset.

Moreover, machine learning models, such as multilayer perceptron neural networks, with their ability to analyze complex and large datasets, significantly increase the speed and accuracy of geophysical analyses. These models provide results that are consistent with observational data and traditional models. The model’s ability to accurately predict changes in the PC index based on input parameters demonstrates its strength in analyzing complex nonlinear relationships within geophysical datasets.

The results indicate that artificial neural network models are powerful tools for predicting and managing geomagnetic disturbances. By processing complex and large datasets, these models significantly improve geophysical analyses and increase prediction accuracy. This can help scientists better understand the complex interactions between solar wind and the magnetosphere and improve predictive models for geomagnetic disturbances.

6 References

Akasofu, S.-I. (1981). Energy coupling between the solar wind and the magnetosphere. *Space Science Reviews*, *28*(2), 121-190.

Beer, C., Reichstein, M., Tomelleri, E., Ciais, P., Jung, M., Carvalhais, N., Rödenbeck, C., Arain, M. A., Baldocchi, D., & Bonan, G. B. (2010). Terrestrial gross carbon dioxide uptake: global distribution and covariation with climate. *Science*, *329*(5993), 834-838.

Boteler, D. H. (2019). A 21st century view of the March 1989 magnetic storm. *Space Weather*, *17*(10), 1427-1441.

dmsp, D. M. S. P. *dmsp*. https://cdaweb.gsfc.nasa.gov/pub/data/dmsp/

Dungey, J. W. (1961). Interplanetary magnetic field and the auroral zones. *Physical Review Letters*, *6*(2), 47.

Feldstein, Y. I., Pisarsky, V. Y., Rudneva, N., & Grafe, A. (1984). Ring current simulation in connection with interplanetary space conditions. *Planetary and space science*, *32*(8), 975-984.

García, S., Luengo, J., & Herrera, F. (2015). *Data preprocessing in data mining* (Vol. 72). Springer.

Gonzalez, W., Joselyn, J.-A., Kamide, Y., Kroehl, H. W., Rostoker, G., Tsurutani, B., & Vasyliunas, V. (1994). What is a geomagnetic storm? *Journal of Geophysical Research: Space Physics*, *99*(A4), 5771-5792.

Goodfellow, I. (2016). Deep learning. In: MIT press.

Han, J., Pei, J., & Tong, H. (2022). *Data mining: concepts and techniques*. Morgan kaufmann.

Hashimoto, K. K., Kikuchi, T., & Ebihara, Y. (2002). Response of the magnetospheric convection to sudden interplanetary magnetic field changes as deduced from the evolution of partial ring currents. *Journal of Geophysical Research: Space Physics*, *107*(A11), SMP 1-1-SMP 1-14.

Holappa, L., & Buzulukova, N. Y. (2022). Explicit IMF B (y) -Dependence of Energetic Protons and the Ring Current. *Geophys Res Lett*, *49*(8), e2022GL098031. https://doi.org/10.1029/2022gl098031

Kan, J., & Lee, L. (1979). Energy coupling function and solar wind-magnetosphere dynamo. *Geophysical Research Letters*, *6*(7), 577-580.

Kivelson, M. G., & Russell, C. T. (1995). *Introduction to space physics*. Cambridge university press.

Kozyra, J., & Nagy, A. (1991). Ring Current Decay Coupling of Ring Current Energy into the Thermosphere/Ionosphere System. *Journal of geomagnetism and geoelectricity*, *43*(Supplement1), 285-297.

Lee, D.-Y., Lyons, L. R., & Yumoto, K. (2004). Sawtooth oscillations directly driven by solar wind dynamic pressure enhancements. *Journal of Geophysical Research: Space Physics*, *109*(A4). https://doi.org/https://doi.org/10.1029/2003JA010246

Maghrabi, A., & Alghamdi, M. (2024). Differential responses of total ozone content to solar activity parameters at two Saudi Arabian locations. *Journal of Atmospheric and Solar-Terrestrial Physics*, *265*, 106379.

O'Brien, T. P., & McPherron, R. L. (2000). An empirical phase space analysis of ring current dynamics: Solar wind control of injection and decay. *Journal of Geophysical Research: Space Physics*, *105*(A4), 7707-7719.

Pfau-Kempf, Y., Papadakis, K., Alho, M., Battarbee, M., Cozzani, G., Pänkäläinen, L., Ganse, U., Kebede, F., Suni, J., & Horaites, K. (2024). Global evolution of flux transfer events along the magnetopause from the dayside to the far tail. *Annales Geophysicae Discussions*, *2024*, 1-28.

Rice, R. C., Chen, L. J., Gershman, D., Fuselier, S. A., Burkholder, B. L., Gurram, H., Beedle, J., Shuster, J., Petrinec, S. M., & Pollock, C. (2024). Dynamics of the storm time magnetopause and magnetosheath boundary layers: An MMS-THEMIS conjunction. *Geophysical Research Letters*, *51*(4), e2023GL106600.

Sedrati, R., Bouchachi, D., & Attallah, R. (2024). Correlation analysis of the long-term interplay of cosmic rays, solar activity, and solar irradiance. *Physica Scripta*, *99*(11), 115032.

Srivastava, N., Hinton, G., Krizhevsky, A., Sutskever, I., & Salakhutdinov, R. (2014). Dropout: a simple way to prevent neural networks from overfitting. *The journal of machine learning research*, *15*(1), 1929-1958.

T. Paul O'Brien, R. L. M. (2000). An empirical phase space analysis of ring current dynamics: Solar wind control of injection and decay. *Journal of Geophysical Research: Space Physics*, *105*(A4), 7707-7719. https://doi.org/https://doi.org/10.1029/1998JA000437

Tepke, B. P. (2019). *Empirical Studies Related to Open Questions Regarding Geomagnetic Storms*. West Virginia University.

Troshichev, O., Janzhura, A., & Stauning, P. (2006). Unified PCN and PCS indices: Method of calculation, physical sense, and dependence on the IMF azimuthal and northward components. *Journal of Geophysical Research: Space Physics*, *111*(A5).

Troshichev, O., Janzhura, A., Troshichev, O., & Janzhura, A. (2012). Solar wind–magnetosphere–ionosphere coupling and the PC index. *Space Weather Monitoring by Ground-Based Means: PC Index*, 77-101.

Troshichev, O., & Sormakov, D. (2019). PC index as a proxy of the solar wind energy that entered into the magnetosphere: 4. Relationship between the solar wind dynamic pressure (PSW) impulses and PC, AL indices. *Journal of Atmospheric and Solar-Terrestrial Physics*, *182*, 200-210.

Troshichev, O. A., & Sormakov, D. A. (2015). PC index as a proxy of the solar wind energy that entered into the magnetosphere: 2. Relation to the interplanetary electric field EKL before substorm onset. *Earth, Planets and Space*, *67*(1), 170. https://doi.org/10.1186/s40623-015-0338-4

Wallace, G. M., Bai, Z., Sadre, R., Perciano, T., Bertelli, N., Shiraiwa, S., Bethel, E. W., & Wright, J. C. (2022). Towards fast and accurate predictions of radio frequency power deposition and current profile via data-driven modelling: applications to lower hybrid current drive. *Journal of Plasma Physics*, *88*(4), 895880401, Article 895880401. https://doi.org/10.1017/S0022377822000708

Wang, C. B., Chao, J. K., & Lin, C.-H. (2003). Influence of the solar wind dynamic pressure on the decay and injection of the ring current. *Journal of Geophysical Research: Space Physics*, *108*(A9). https://doi.org/https://doi.org/10.1029/2003JA009851

Yamamoto, K., Seki, K., Amano, T., Nakamizo, A., Miyoshi, Y., & Yamakawa, T. (2024). A drift kinetic simulation of internally driven ULF waves based on multi-point spacecraft observations in the ionosphere and the magnetosphere.